Neuron
Article

Cdk5rap2 Interacts with Pericentrin to Maintain the Neural Progenitor Pool in the Developing Neocortex

Joshua J. Buchman,[1,2,3] Huan-Chung Tseng,[1] Ying Zhou,[1,2] Christopher L. Frank,[1,2] Zhigang Xie,[5] and Li-Huei Tsai[1,2,4,*]
[1]Department of Brain and Cognitive Sciences, Picower Institute for Learning and Memory, Massachusetts Institute of Technology, 77 Massachusetts Avenue, Building 46, Room 4235A, Cambridge, MA 02139, USA
[2]Howard Hughes Medical Institute, 77 Massachusetts Avenue, Building 46, Room 4235A, Cambridge, MA 02139, USA
[3]Program in Neuroscience, Harvard Medical School, Boston, MA 02115, USA
[4]Stanley Center for Psychiatric Research, Broad Institute of Harvard and Massachusetts Institute of Technology, Cambridge, MA 02139, USA
[5]Department of Neurosurgery, Department of Pharmacology and Experimental Therapeutics, Boston University School of Medicine, Boston, MA 02118, USA
*Correspondence: lhtsai@mit.edu
DOI 10.1016/j.neuron.2010.03.036

SUMMARY

Primary autosomal-recessive microcephaly (MCPH) and Majewski osteodysplastic primordial dwarfism type II (MOPDII) are both genetic diseases that result in decreased brain size at birth. MCPH is thought to arise from alterations in the size of the neural progenitor pool, but the cause of this defect has not been thoroughly explored. We find that one of the genes associated with MCPH, *Cdk5rap2*, is highly expressed in the neural progenitor pool and that its loss results in a depletion of apical progenitors and increased cell-cycle exit leading to premature neuronal differentiation. We link Cdk5rap2 function to the pericentriolar material protein pericentrin, loss of function of which is associated with MOPDII. Depletion of pericentrin in neural progenitors phenocopies effects of Cdk5rap2 knockdown and results in decreased recruitment of Cdk5rap2 to the centrosome. Our findings uncover a common mechanism, involving aberrations in the neurogenesis program, that may underlie the development of microcephaly in multiple diseases.

INTRODUCTION

Neurogenesis occurs in the developing mouse cortex during a 9 day period, starting at embryonic day 11 (E11). The developing cortex can be divided into the ventricular zone (VZ), subventricular zone (SVZ), intermediate zone (IZ), and cortical plate (CP). Neural progenitors reside in the VZ and SVZ, where they divide to produce immature neurons. These migrate through the IZ before coming to rest in the CP, where they fully differentiate.

The centrosome is the organelle responsible for nucleating and organizing the majority of microtubule structures in animal cells. It plays a central role in multiple processes important to corticogenesis. Altered protein expression that weakens the microtubule link between the centrosome and oscillating nuclei can disrupt interkinetic nuclear migration and alter neurogenesis (Xie et al., 2007). In dividing cells, the centrosome helps organize the mitotic spindle and the astral microtubules (Busson et al., 1998; Doxsey, 2001; Faulkner et al., 2000; Yingling et al., 2008). The centrosome also plays a key role in neuronal migration to the CP (Higginbotham and Gleeson, 2007; Tsai and Gleeson, 2005; Xie et al., 2003). Migrating neurons transition through a multipolar phase during which axonal specification occurs, and this process may also depend on centrosome orientation (de Anda et al., 2005; Zmuda and Rivas, 1998).

Altered expression of several proteins with centrosomal localization is associated with manifestation of autosomal-recessive primary microcephaly (MCPH) (Woods et al., 2005; Zhong et al., 2006). MCPH is a nonprogressive disorder typified by a head circumference (HC) that ranges between 3 and 14 standard deviations below the mean value for individuals of a given sex and age (Aicardi, 1998; Roberts et al., 2002; Woods et al., 2005). Differences in HC are detectable by the seventh month of gestation (Aicardi, 1998; Desir et al., 2008). The most significant reduction is apparent in the cerebral cortex (Bond et al., 2002). Central nervous system (CNS) architecture appears grossly normal, but cortical gyri patterning is simplified (Bond et al., 2002; Desir et al., 2008). The fact that MCPH is detectable during fetal development, is nonprogressive, and has a major effect on the cortex suggests that it manifests itself through a deficiency in proliferation of cortical neural progenitor cells. MCPH has been linked to eight genetic loci and five known genes (Jackson et al., 1998; Jamieson et al., 2000, 1999; Kumar et al., 2009; Leal et al., 2003; Moynihan et al., 2000; Pattison et al., 2000; Roberts et al., 1999). All of these play a role in centrosome-associated functions (Cox et al., 2006; Fong et al., 2008; Pfaff et al., 2007).

Our study sought to determine the role of one of these proteins, Cdk5rap2, in mammalian corticogenesis. Cdk5rap2 helps maintain centrosome cohesion, recruits γTuRC to the centrosome, and facilitates formation of spindle astral microtubules (Fong et al., 2008; Graser et al., 2007). The Cdk5rap2 transcript is detectable in developing structures and proliferative regions of

the embryonic and postnatal mammalian brain, including the cerebral cortex, suggesting a role in neural progenitor proliferation (Bond et al., 2005; Magdaleno et al., 2006). Mutations that result in premature *Cdk5rap2* stop codons are associated with MCPH (Bond et al., 2005; Hassan et al., 2007).

Another centrosome protein, pericentrin, has been linked to microcephalic osteodysplastic primordial dwarfism type II (MOPD II), a syndrome characterized by microcephaly, intrauterine and postnatal growth retardation, and skeletal abnormalities (Majewski et al., 1982; Rauch et al., 2008). Pericentrin localizes to the PCM and functions in ciliogenesis, centrosomal γTuRC recruitment, and mitotic spindle assembly (Doxsey et al., 1994; Jurczyk et al., 2004; Zimmerman et al., 2004).

To obtain insights into the mechanisms underlying MCPH, we sought to examine the role of Cdk5rap2 in corticogenesis. We examined the expression of Cdk5rap2 in the developing cortex and confirm its expression in neural progenitors, where it localizes to the centrosome. Small hairpin-mediated knockdown of Cdk5rap2 starting at E11.5 resulted in a redistribution of cells between cortical zones, with more cells exiting the cell cycle and differentiating into neurons. There was also a change in the makeup of the progenitor pool following knockdown, with fewer apical progenitors and more basal progenitors comprising the overall pool. Interestingly, we observed a functional association of Cdk5rap2 with pericentrin, wherein pericentrin recruits Cdk5rap2 to the centrosome to support its critical role in the maintenance of the progenitor pool during corticogenesis. Together, these findings reveal a functional relationship between two centrosome proteins that regulate neurogenesis with important implications for the manifestation of diseases characterized by microcephaly.

RESULTS

Expression of Cdk5rap2 in the Developing Neocortex and Subcellular Localization

The microcephaly phenotype that is the hallmark of MCPH is postulated to arise through deviations in the normal proliferative program of neural progenitors that occurs during corticogenesis. We therefore wanted to examine the expression pattern of Cdk5rap2 in the developing cortex. To do so, we generated a Cdk5rap2 antibody that recognizes the Cdk5rap2 amino-terminus. Purified antibody specifically detected full-length flag-tagged Cdk5rap2 (see Figure S1A available online).

In order to examine the time course of Cdk5rap2 expression in the developing mouse brain, we prepared whole-brain extracts at different ages. Cdk5rap2 was detectable at E9.5 as a band greater than 200 kDa (Figure 1A). This band peaked in intensity between E10.5 and E13.5, remained robust at E15.5, and declined thereafter. We also detected a doublet of ~90 kDa in extracts beginning at E13.5 that increased in intensity through P7.5, mirroring the decline of the larger species. This doublet may represent alternative Cdk5rap2 isoforms. We conclude that Cdk5rap2 is expressed in the developing brain and that its expression peaks during periods of active neurogenesis in the developing neocortex.

To examine the spatial expression pattern of Cdk5rap2 in the developing neocortex, we probed coronal neocortical sections from mouse embryos harvested at E14.5. Cdk5rap2 antibody displayed a punctate staining pattern apparent in all cortical layers (Figure 1B, bottom). Cdk5rap2 signal was detectable in Tuj1-positive neurons of the embryonic cortical plate (Figure S2B). We observed the most intense signal at the luminal surface of the VZ. This signal was punctate and present in the apical endfeet of nestin-positive progenitors (Figures 1B, bottom right panel, and 1C). Cdk5rap2 puncta overlapped almost completely with those of the centrosome protein pericentrin in images of the ventricular surface, demonstrating that our antibody detects a true centrosome signal (Figure 1D). Cdk5rap2 signal was also detectable in nestin-positive cultured neural progenitors where it colocalized with centrosome proteins (Figure S2C). We conclude that Cdk5rap2 is expressed in nestin-positive neural progenitor cells of the developing neocortex during neurogenesis, and that it localizes to the centrosome.

Knockdown of Cdk5rap2 Results in Altered Cell Distribution in the Developing Neocortex

In order to determine what role Cdk5rap2 plays in neurogenesis, we developed and screened small hairpin expression constructs capable of targeting *Cdk5rap2* transcript. We identified three different small hairpin constructs (shC1, shC2, and shC3) capable of knocking down expression of green fluorescent protein (GFP)-tagged Cdk5rap2, endogenous Cdk5rap2 in cultured cell lines, and in utero electroporated cells in brain slices (Figure S2).

We coelectroporated cells of the dorsal cortex with a GFP-expression plasmid as well as one of the small hairpin constructs at day E11.5 and harvested embryos 72 hr later, at E14.5. We then analyzed the distribution of GFP-positive cells between different zones of the developing neocortex. The majority of cells were found in either the IZ or CP, but a sizable population remained in the VZ and SVZ (Figures 2A and 2B). Knockdown of Cdk5rap2 resulted in a significant alteration in cell distribution between cortical zones. Specifically, knockdown resulted in significantly fewer cells remaining in the VZ/SVZ (group, n; control, n = 6; shC1, n = 7; shC2, n = 6; shC3, n = 3) and more cells entering the IZ or CP. Coelectroporation of a Cdk5rap2 construct resistant to shC2-mediated knockdown (Cdk5rap2res) and shC2 was able to restore cellular distribution to approximately control values (control + vector, n = 3; shC2 + vector, n = 4; shC2 + Cdk5rap2res, n = 4) (Figure S4). In order to determine whether this redistribution of cells was a transient effect of knockdown, we also performed in utero electroporation with control hairpin or shC2 and harvested electroporated brains at E17.5. We found that the effect of Cdk5rap2 on cell distribution was more pronounced following a further 72 hr of small hairpin expression (Figures 2C and 2D). A significantly larger fraction was found in the IZ and CP following Cdk5rap2 knockdown (control and shC2, n = 3). Moreover, the VZ/SVZ was virtually cleared of cells in the knockdown group (Figure 2C, far right panel).

Knockdown of Cdk5rap2 Results in Increased Neuronal Differentiation

Following cell-cycle exit in the VZ and SVZ, cells generally migrate to the CP. Migration takes place simultaneously with the process of neuronal differentiation. To determine whether

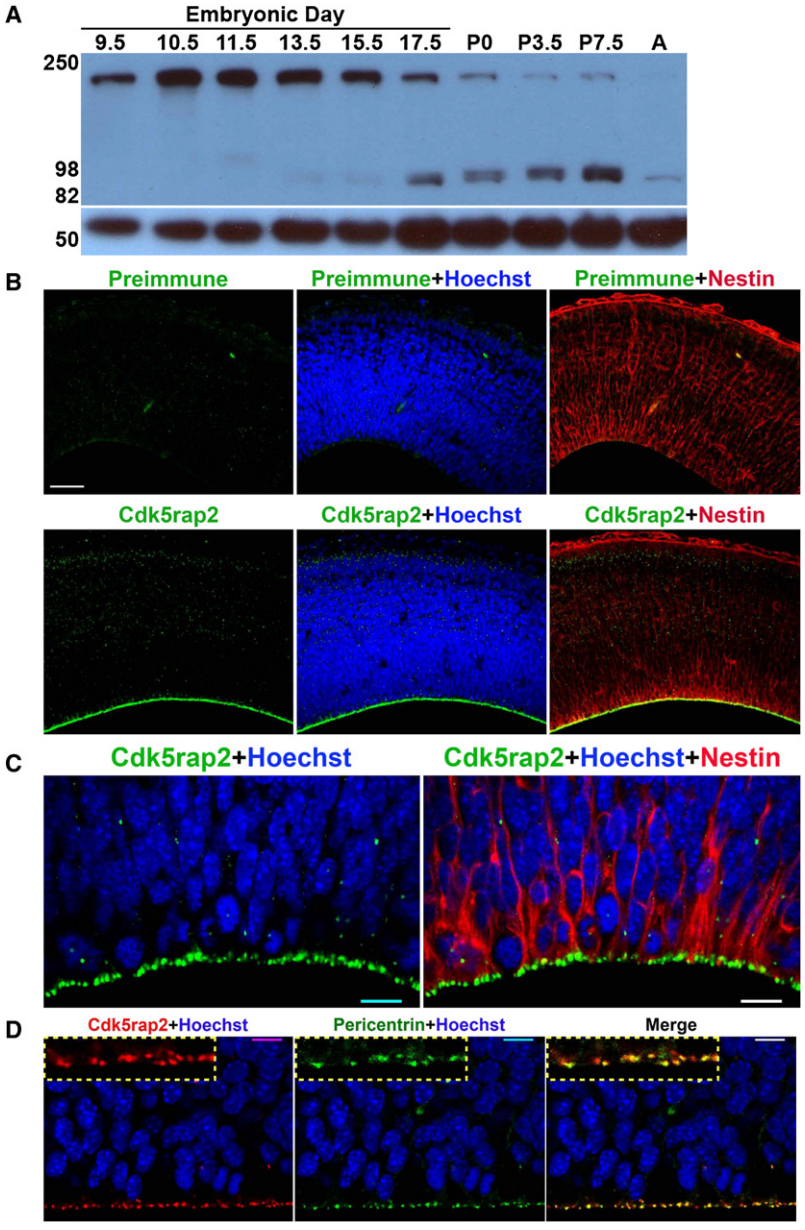

Figure 1. Cdk5rap2 Expression in the Developing Brain

(A) Developmental time course of Cdk5rap2 expression in brain. Numbers above each lane indicate the embryonic or postnatal (P) day extract was collected. A indicates adult brain extract. Upper blot, Cdk5rap2. Lower blot, alpha tubulin.

(B) Neocortical brain sections were probed with either preimmune serum (upper panels) or Cdk5rap2 antibody (lower panels). Panels: Preimmune or Cdk5rap2 signal alone (left panels) or merged with Hoechst (middle panels) or nestin (right panels). Scale bar = 50 μm.

(C) High-magnification image of neocortical sections taken at the apical edge of the VZ, showing Cdk5rap2 expression in nestin-positive neural progenitors. Left panel: Cdk5rap2 and Hoechst. Right panel: Merge of left panel with nestin. Scale bar = 10 μm.

(D) High-magnification image taken at the interface of the VZ and lateral ventricle (bottom), displaying overlap of Cdk5rap2 with pericentrin. Left panel: Cdk5rap2 and Hoechst. Middle panel: Pericentrin and Hoechst. Right panel: Merge of Cdk5rap2, pericentrin, and Hoechst signals. Inset shows zoom view of apical VZ edge. Scale bar = 10 μm.

the redistribution of cells we observed is correlated with cell differentiation we stained for the neuronal marker Tuj1. In control brains, most electroporated cells were found in regions of the cortex that robustly expressed Tuj1. However, a noticeable portion were located in the Tuj1− region of the VZ (Figure 3A, top row). Following Cdk5rap2 knockdown, a significantly larger portion of cells were found in Tuj1$^+$ regions of the cortex, and many cells in the VZ expressed Tuj1 (Figures 3A and 3C; control, shC1, shC2, and shC3, n = 3). Additionally, coexpression of shC3 and a GFP expression plasmid regulated by a NeuroD promoter (pNeuroD-GFP) indicated that significantly more electroporated cells were at a postmitotic stage compared with controls (Figure S4; control and shC3, n = 3). These observations indicate that knockdown of Cdk5rap2 levels results in an increased propensity for neurons to differentiate.

The CP is formed in an inside-out manner, with early-born neurons situated in the deeper layers (Angevine and Sidman, 1961). FoxP2 is a marker of layer 6 neurons, and is first visible in the neocortex at E14.5 (Ferland et al., 2003). Based on the fact that we observed increased Tuj1 costaining and fewer GFP$^+$ cells in the VZ/SVZ at E14.5 following Cdk5rap2 knockdown, we hypothesized that we should observe an increase in neurons born at this stage following knockdown. We therefore quantified the fraction of GFP$^+$ cells in the IZ and CP (i.e., the postmitotic population) that costained for FoxP2 at E17.5. We found that a significantly larger fraction of this cell population expresses FoxP2 after knockdown (Figures 3E and 3F; control and shC2, n = 3). Additionally, we quantified GFP$^+$ cell distribution across neuronal layers at P6 (Figures 3B and 3D). We found that in Cdk5rap2 knockdown samples a significantly larger fraction of the total GFP$^+$ cell population was located in layer 6, a significantly smaller fraction was found in layer 5, and there was a trend toward a smaller fraction being found in layer 2/3 and 4 compared with controls (control and shC2, n = 4). Thus, we conclude that Cdk5rap2 knockdown results in an increased propensity for cells to differentiate into neurons at early time points during corticogenesis.

We also asked whether increased neuronal differentiation is a property restricted to cells exposed to Cdk5rap2 knockdown at early time points, or whether Cdk5rap2 knockdown continues to influence the differentiation of actively cycling cells at later time points. To investigate this possibility, we performed in utero electroporation surgery, and at E14.5 we pulse labeled the actively cycling progenitors in electroporated brains

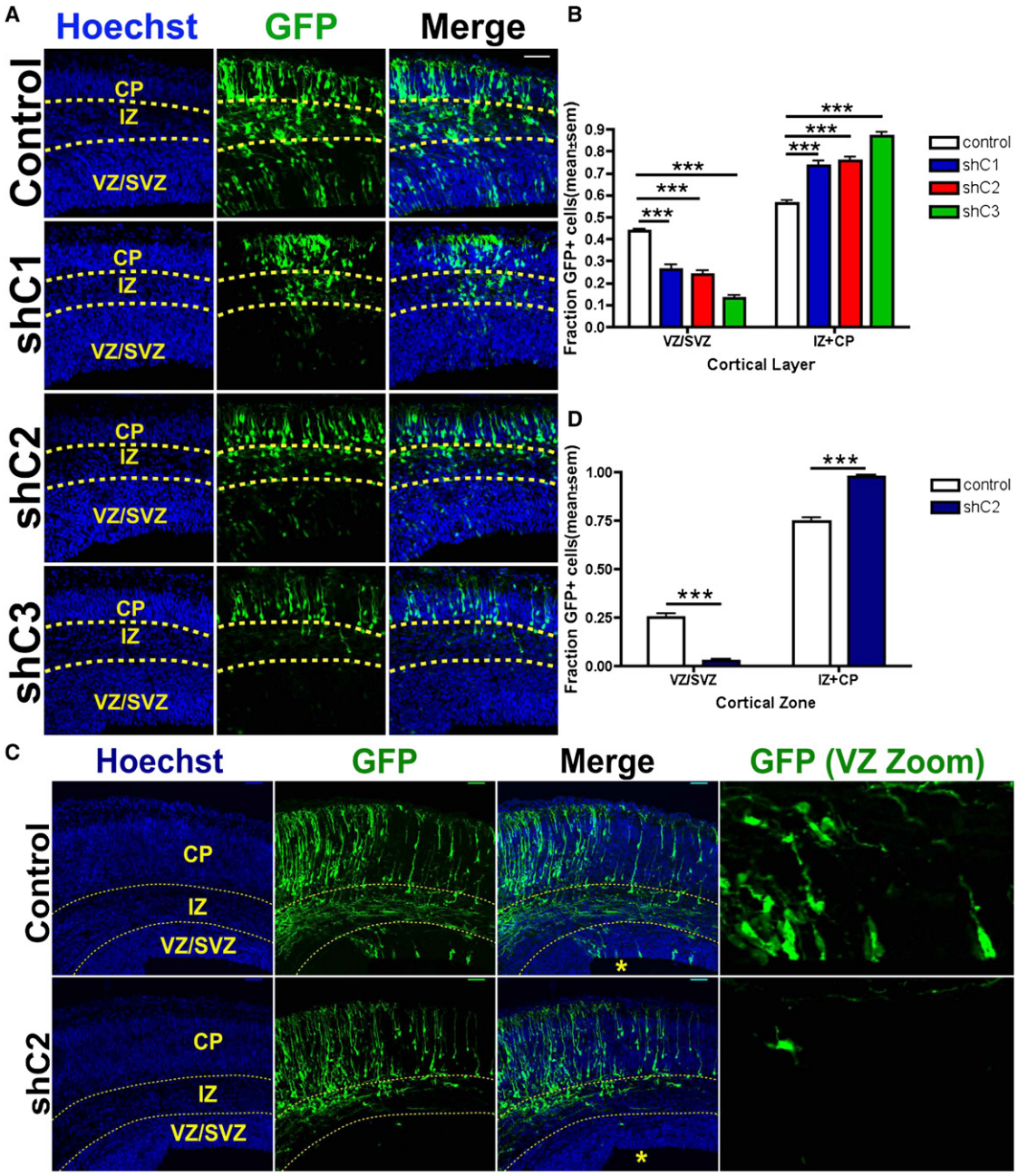

Figure 2. Cdk5rap2 Depletion Results in Altered Cell Distribution across Cortical Layers

(A) Images of GFP$^+$ cell distribution in E14.5 neocortex, 72 hr postelectroporation. Left column: Hoechst signal. Middle column: GFP signal. Right column: Merge of Hoechst and GFP signals. Top row: Random sequence control electroporated brain section. Lower rows: Cdk5rap2 small hairpins shC1, shC2, and shC3 electroporated brain sections from top to bottom, respectively.

(B) Quantification of GFP$^+$ cell distribution between VZ/SVZ and IZ + CP zones at E14.5. Data are mean and standard error of the mean (±SEM); ***$p < 0.0001$, one-way analysis of variance (ANOVA).

(C) Images of GFP$^+$ cell distribution in E17.5 neocortex, 6 days postelectroporation. Left column: Hoechst. Middle column: GFP. Right column: Merge of Hoechst and GFP. Far right column: Zoom image of region directly above yellow star in merge column, showing cells in VZ/SVZ. Top row: Control brain sections. Bottom row: shC2 brain section.

(D) Quantification of GFP$^+$ cell distribution between VZ/SVZ and IZ + CP zones at E17.5. Mean ± SEM; ***$p = 0.0005$, t test. Letters in images denote different cortical zones. Dashed lines denote borders between different cortical zones. All scale bars represent 50 μm.

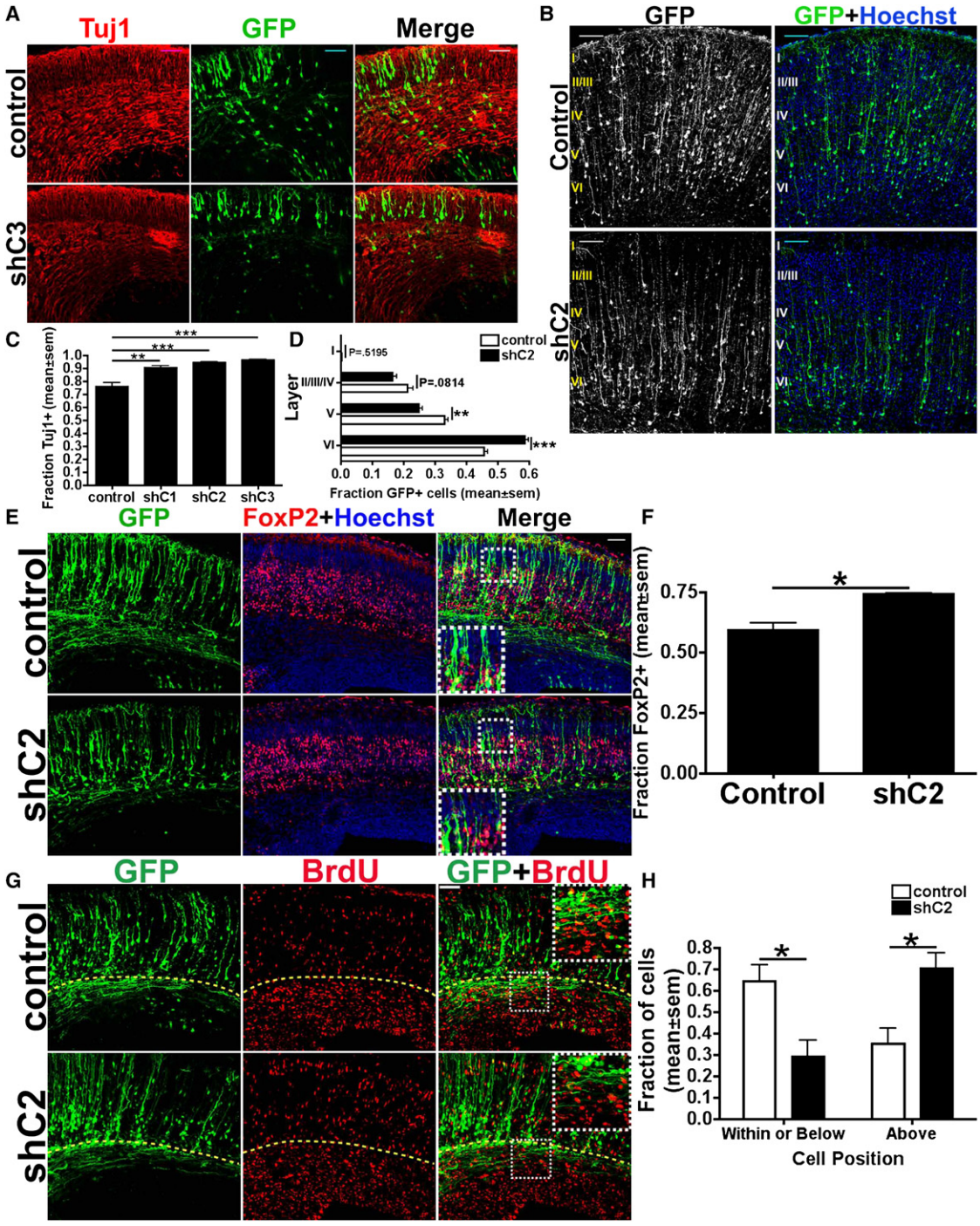

Figure 3. Cdk5rap2 Depletion Results in Increased Premature Neuronal Differentiation

(A) Images of GFP$^+$ cells and overlap with Tuj1 staining in E14.5 brains. Left column: Tuj1. Middle column: GFP. Right column: Merge. Top row: Control. Bottom row: shC3 brain section.

(B) Images of P6 electroporated brain sections. Left column: GFP. Right column: GFP merge with Hoechst. Top row: Control. Bottom row: shC2 brain section. Roman numerals indicate location of neuronal layers.

(C) Quantification of fraction of GFP$^+$ cells that overlap with Tuj1 signal. Mean ± SEM; one-way ANOVA.

(D) Quantification of distribution of GFP$^+$ cells across neuronal layers at P6. Mean ± SEM; t test.

(E) Images of GFP$^+$ cell overlap with FoxP2 signal at E17.5. Left column: GFP. Middle column: FoxP2 and Hoechst. Right column: Merge. White boxes show zoom image. Top row: control. Bottom row: shC2 brain section.

(F) Quantification of overlap between GFP$^+$ cells and FoxP2 signal in the IZ and CP only. Mean ± SEM; t test.

by 5-bromo-2-deoxyuridine (BrdU) injection into pregnant dams. We then waited a further 72 hr before quantifying the distribution of BrdU-labeled GFP-positive cells within the cortex. The corticothalamic and corticofugal axon tracts serve as an approximate border between the IZ and the CP. Progenitor cells reside in the VZ and SVZ while recently differentiated neurons are found in the IZ. The CP consists of neurons that have either finished migrating or are completing radial migration. In order to obtain an idea of how Cdk5rap2 knockdown affects differentiation of actively cycling progenitors at the E14.5 time point, we examined the distribution of the BrdU, GFP double-positive cell population between the region below and within the axon tracts and the region above the upper border of the axon tracts (Figure 3G). We found that at E17.5 fewer BrdU-labeled cells remained in the proliferative and transitional IZ regions below the upper border of the axon tracts region (control and shC2, n = 3) and significantly more BrdU-labeled cells were positioned above the axon tracts region compared to control samples (Figure 3H). This demonstrates that Cdk5rap2 knockdown results in increased neuronal differentiation of neural progenitor cells even at relatively later stages of neurogenesis.

Knockdown of Cdk5rap2 Results in Increased Cell-Cycle Exit and Decreased Cell Proliferation

Progenitor cells of the embryonic neocortex are actively cycling cells that can give rise to both immature neurons and more progenitors. Newly born neurons undergo neuronal differentiation while progenitor daughters reenter the cell cycle. Because knockdown of Cdk5rap2 increased the observed level of neuronal differentiation, we asked whether this increase coincided with changes in proliferative activity. We performed in utero electroporation and injected pregnant dams with BrdU at E13.5. We then harvested electroporated brains at E14.5 and determined the 24 hr BrdU-labeling index within the GFP-positive cell population (Figures 4A and 4B). Knockdown of Cdk5rap2 led to a significant decrease in the 24 hr BrdU-labeling index compared to controls (all conditions, n = 3). The decrease we observed indicates that fewer cells passed through a single S phase following Cdk5rap2 knockdown, indicative of decreased cell-cycle activity.

We also costained the same sections for Ki-67 in order to mark the actively proliferating cell population (Figure 4A, column iii), and determined the cell-cycle exit index (Figure 4C). Cdk5rap2 knockdown resulted in a significant increase in cell-cycle exit compared with controls (all conditions, n = 3). Thus, depletion of Cdk5rap2 results in increased cell-cycle exit, consistent with a decrease in cell proliferation.

We also stained electroporated brains with the mitotic marker phosphohistone H3 (PHH3) (Figure 4D). Cdk5rap2 knockdown correlated with a significantly lowered mitotic index at this stage as assessed by PHH3 overlap with GFP (Figure 4E, all conditions, n = 3). Taken together, these observations demonstrate that Cdk5rap2 depletion results in reduced proliferative activity and a concomitant increase in cell-cycle exit. We did not observe any increase in cleaved caspase 3 (CC3) staining following Cdk5rap2 knockdown, excluding apoptosis as an explanation for the phenotypes we observed (Figure S5).

Cdk5rap2 Knockdown Alters the Makeup of the Progenitor Pool and Cell-Cycle Parameters

When we examined the position of individual mitotic events, we found that more cells in the mitotic population mitosed away from the ventricular surface following Cdk5rap2 knockdown compared with controls (Figure S6A; control and shC2, n = 5). One potential explanation for this change is an alteration in the makeup of the neural progenitor pool as apical progenitors normally divide at the ventricular surface whereas basal progenitors are prone to divide at more basal positions (Farkas and Huttner, 2008). We examined the makeup of the progenitor pool in control and Cdk5rap2 knockdown conditions at E14.5 and found that knockdown led to a significant decrease in the proportion of apical progenitors identified by Pax6 (Figures 5A and 5B; control and shC2, n = 3) and a significant increase in the proportion of basal progenitors identified by Tbr2 (Figures 5C and 5D; control and shC2, n = 6). Endfeet of apical progenitors following knockdown appeared grossly normal, and we did not identify any obvious defects in localization or expression of several apical polarity markers (Figure S6G). Thus, Cdk5rap2 levels modulate the makeup of the progenitor pool, providing an explanation for the increased cell-cycle exit and neuronal differentiation observed following knockdown.

We also found that Cdk5rap2 knockdown had significant effects upon cell-cycle dynamics. We observed that knockdown of Cdk5rap2 in Neuro-2A (N2A) cells (Figure S6B) resulted in a significant shift in the proportion of cells to the G0/G1 population from the S phase population (Figure S6D; T cell receptor coreceptor CD8 negative control small hairpin (CD8), n = 4; shC1, n = 4; shC2, n = 3). We also found that the 1 hr BrdU labeling index in N2A cells was decreased following knockdown (Figure S6E; control, n = 4; shC1, n = 4; shC2, n = 3) as was the 2 hr BrdU labeling index in cultured neural progenitors (Figures S6C and S6F; CD8, n = 10; shC1, n = 10; shC2, n = 7). These results also suggest that Cdk5ap2 knockdown increases overall cell-cycle length, possibly by increasing G1 duration. Thus, Cdk5rap2 knockdown may result in increased neurogenesis at early time points and depletion of the neural progenitor pool by altering a key determinant of cell-cycle exit or re-entry (i.e., G1 length; see Discussion).

Cdk5rap2 Interacts with Pericentrin through Defined Protein Domains

We next attempted to determine the molecular mechanism by which Cdk5rap2 regulates neurogenesis. In order to do so, we performed a mass-spectrometry-based interaction screen of

(G) Images of BrdU-labeled GFP$^+$ cells in electroporated E17.5 brain slices. Left column: GFP. Middle column: BrdU. Right column: Merge. Top row: Control electroporated brain section. Bottom row: shC2 electroporated brain section. Dashed yellow lines indicate upper border of axon tracts. White boxes show zoom image.

(H) Quantification of distribution of BrdU labeled GFP$^+$ cell population. Within or below = fraction of GFP$^+$, BrdU$^+$ cells located below or within the axon tracts region. Above = fraction of GFP$^+$, BrdU$^+$ cells located above the upper border of the axon tracts region. Mean ± SEM; t test.

For all graphs: *$p < 0.05$; **$p < 0.01$; ***$p < 0.001$. Panels (A), (E), and (G) scale bars = 50 μm. Panel (B) scale bar = 100 μm.

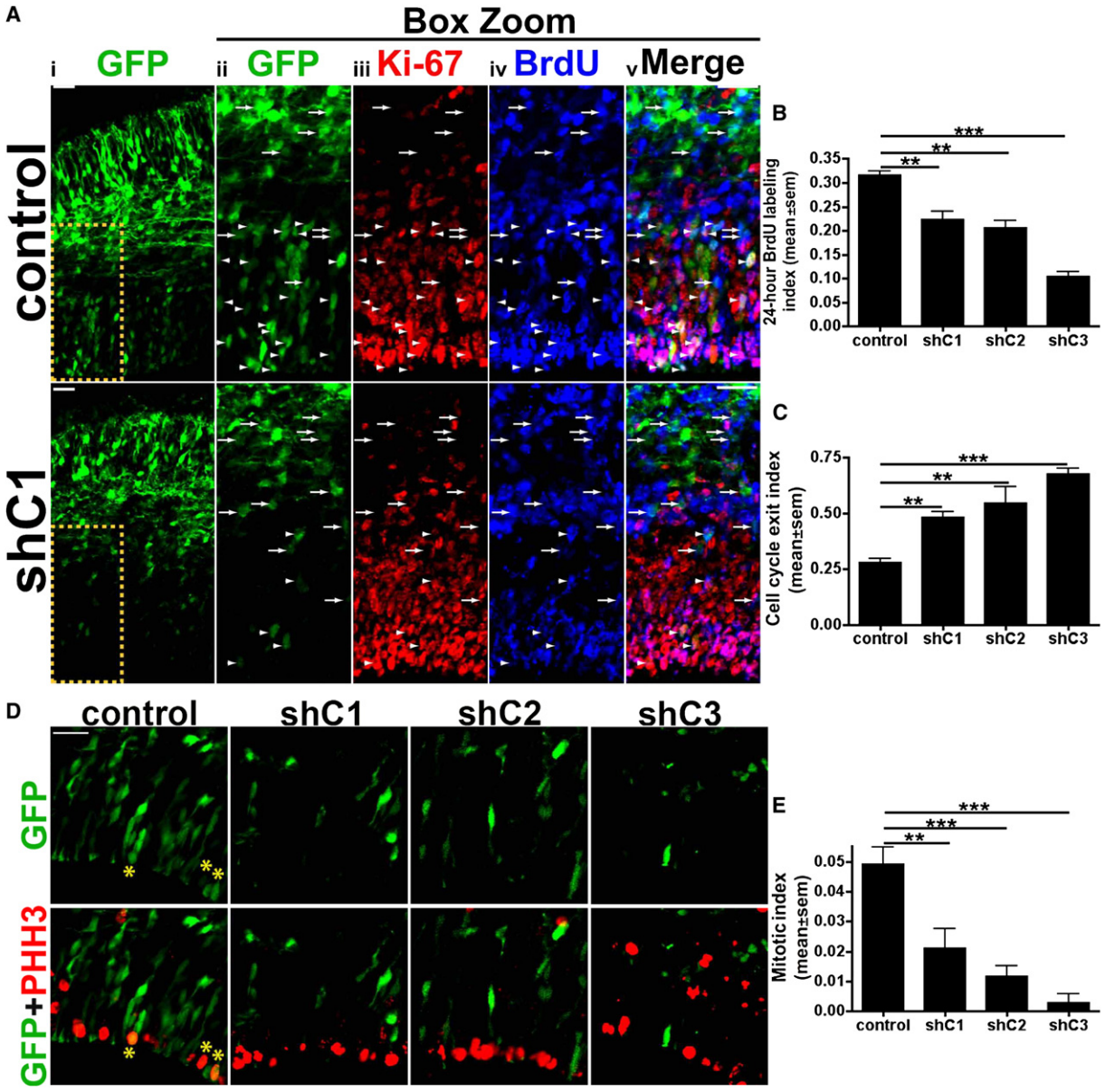

Figure 4. Cdk5rap2 Depletion Results in Decreased Cell Proliferation and Increased Cell-Cycle Exit

(A) Images of electroporated brain slices at E14.5 stained for GFP, Ki-67, and BrdU. Column i: Image of GFP signal from brain slice including complete expanse from ventricular surface (bottom) to pial surface (top). Hatched yellow boxes denote zoomed area shown in panels of columns ii-v. Column ii: GFP. Column iii, Ki-67. Column iv, BrdU. Column v: merge of columns ii-iv. Top row: Control. Bottom row: shC1. Arrowheads indicate GFP, Ki-67, BrdU triple-positive cells. Arrows indicate GFP, BrdU double-positive cells.

(B) Quantification of 24 hr BrdU labeling index.

(C) Quantification of cell-cycle exit index.

(D) Images of cells in the VZ at E14.5 stained for GFP and PHH3. Top row: GFP. Bottom row: Merge of GFP and PHH3. Yellow asterisks indicate GFP, PHH3 double-positive cells. Left column: Control. Right columns: shC1, shC2, and shC3 from left to right, respectively.

(E) Quantification of mitotic index.

For all graphs: mean ± SEM; $^{**}p < 0.01$; $^{***}p < 0.001$; one-way ANOVA. All scale bars = 25 μm.

proteins coimmunoprecipitated by our Cdk5rap2 antibody from E11.5 mouse brain. Immunoprecipitation by Cdk5rap2 antibody yielded five visible bands that were analyzed by mass spectrometry (labels 1 through 5 in Figure 6A and Table 1). Four of these bands (2 through 5) contained protein sequence that matched that of Cdk5rap2. These bands most likely represent full-length Cdk5rap2 and either other isoforms of Cdk5rap2 or degraded protein fragments.

Our screen only identified one other unique coimmunoprecipitated protein, probably due to the fact that we used harsh

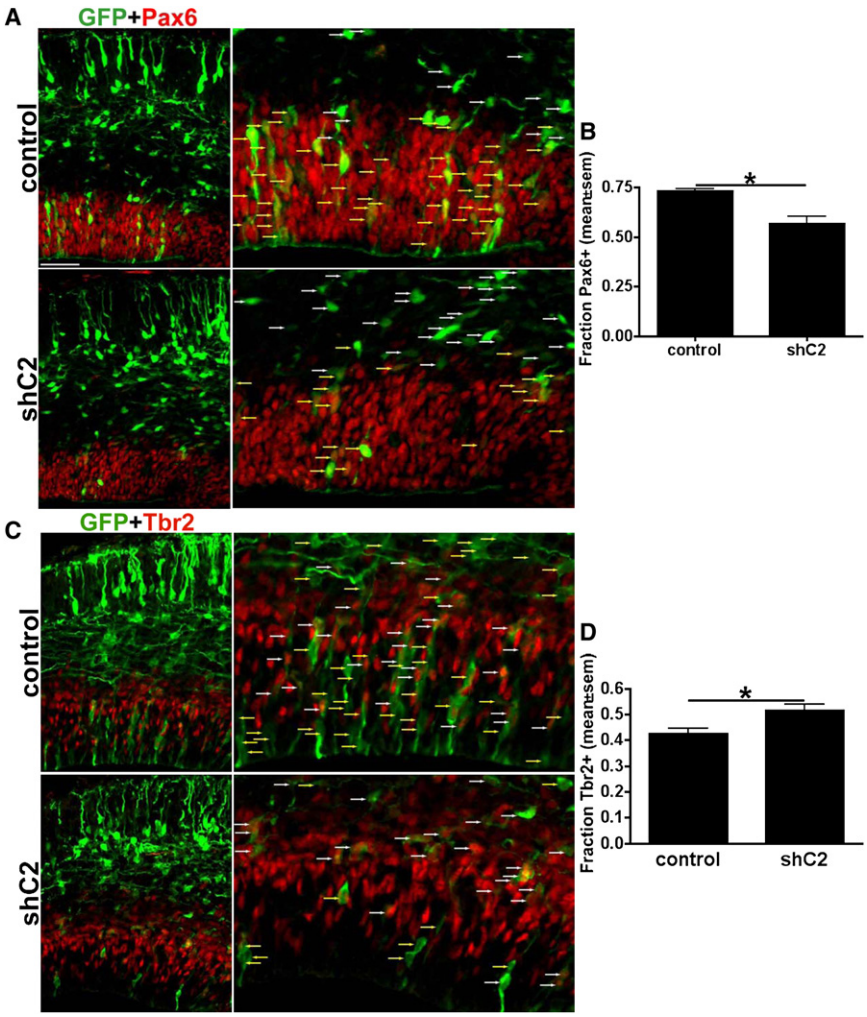

Figure 5. Cdk5rap2 Depletion Alters the Makeup of the Progenitor Pool

(A) Images of electroporated brain sections stained for Pax6 (red) and GFP (green). Top, control; bottom, shC2; left column, full view of brain sections from ventricular to pial surface; right column, zoom box of VZ/SVZ. White arrows, GFP^+ cells; yellow arrows, GFP^+,$Pax6^+$ cells.

(B) Quantification of fraction of GFP^+ cells that are also $Pax6^+$.

(C) Images of electroporated brain sections stained for Tbr2 (red) and GFP (green). Top, control; bottom, shC2; left column, full view of brain sections from ventricular to pial surface; right column, zoom box of VZ/SVZ. White arrows, GFP^+,$Tbr2^+$ cells; yellow arrows, GFP^+ cells.

(D) Quantification of fraction of GFP^+ cells that are also $Tbr2^+$.

All graphs: mean ± SEM; *p < .05; t test. Scale bar = 50 μm.

extraction conditions to maximize the efficiency of Cdk5rap2 extraction. Analysis of band number 1 matched the protein sequence of pericentrin (Table 1). An interaction between Cdk5rap2 and pericentrin was potentially interesting because both proteins are implicated genetic conditions in humans characterized in part by microcephaly.

In order to confirm the validity of the Cdk5rap2-pericentrin interaction, we used a second cell-based system. We found that a Flag-tagged full-length Cdk5rap2 (Flag-Cdk5rap2) was capable of coimmunoprecipitation (coIP) of endogenous pericentrin from cultured N2A cells (Figure 5B). Empty Flag vector did not give this result, nor did Flag-tagged ATF4, demonstrating specificity of the co-IP of pericentrin by Cdk5rap2. Interestingly, while Flag-Cdk5rap2 was able to coIP some pericentrin A, it seemed to interact with the larger pericentrin B isoform more strongly (Figure 6B).

To determine which domains of Cdk5rap2 and pericentrin mediate their interaction, we produced Flag-tagged Cdk5rap2 constructs comprising different domains of Cdk5rap2 (Figure S7A). Analysis showed that only the final 622 carboxy-terminal amino acid residues of Cdk5rap2 were necessary for coIP of pericentrin (Figures S7A and S7B). To more accurately define the domain of Cdk5rap2 necessary for coIP of pericentrin we synthesized constructs containing subdomains of this portion of Cdk5rap2 (Figure 6C). Whereas constructs composed of the entire Cdk5rap2 sequence except this domain (1-1553) or the more amino-terminal portion of this domain (construct 6a) did not coimmunoprecipitate pericentrin, constructs containing only this domain (construct 6) or the extreme carboxy terminal portion of Cdk5rap2 (construct 6b) were capable of pericentrin coIP (Figures 6C and 6E). This demonstrates that the interaction between Cdk5rap2 and pericentrin is mediated through the extreme carboxy terminal portion of Cdk5rap2. Again, in most experiments, Cdk5rap2 constructs coimmunoprecipitated the larger pericentrin B isoform more strongly than lower isoforms, suggesting that the interaction between Cdk5rap2 and pericentrin is biased toward this isoform.

We then mapped the domain of pericentrin that interacts with Cdk5rap2, using plasmids that express non-overlapping hemagglutinin (HA)-tagged fragments of the pericentrin protein sequence (constructs 1 through 10, Figure 6D). Only construct 7 allowed strong co-IP of Cdk5rap2 (Figure 6F). Interestingly, the pericentrin domain expressed by construct 7 overlaps the border of pericentrin B and the carboxy terminus of the pericentrin A protein sequence (dashed line, Figure S7C). To determine whether the Cdk5rap2 binding domain lies exclusively within the pericentrin B sequence, we constructed pericentrin fragment expression constructs capable of expressing only the carboxy terminus of pericentrin A (construct 7a), a sequence spanning the border of the pericentrin A and B sequences (construct 7b), and a sequence consisting of only the pericentrin B sequence expressed by fragment 7 (construct 7c, Figure S7C). Only

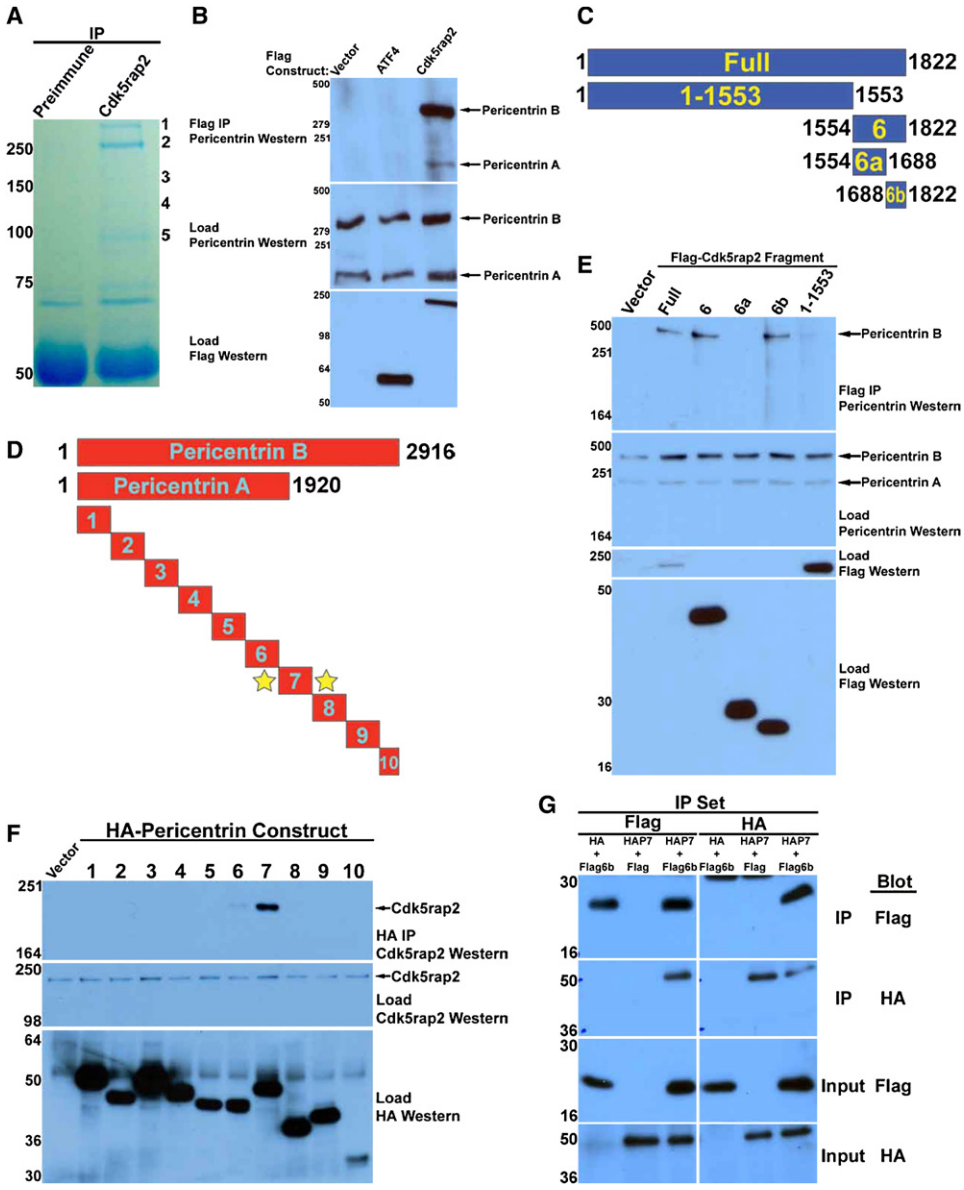

Figure 6. Cdk5rap2 and Pericentrin Interact through Specific Protein Domains

(A) Image of Coomassie-stained gel containing protein bands immunoprecipitated by Cdk5rap2 antibody. Five gel bands (labeled 1 through 5) were analyzed by mass spectrometry (Table 1).

(B) Pericentrin coIP by Cdk5rap2. N2A cells transfected with Flag vector (Vector), Flag-tagged ATF4 (ATF4), or Flag-tagged Cdk5rap2 (Cdk5rap2) were lysed, and extracts were subjected to Flag bead IP followed by pericentrin western blot (top). Middle: Pericentrin western of whole-cell extract. Bottom: Flag western of whole-cell extract. Labels to the right identify endogenous pericentrin A and B isoforms.

(C) Diagram of Cdk5rap2 constructs used in (E) and their location within the full-length (Full) amino acid sequence. Yellow labels indicate construct name and correspond to lane labels in (E). Black numbers indicate beginning and ending amino acid residues comprising each construct with respect to the full-length amino acid sequence.

(D) Diagram of pericentrin A and B and the domain fragments used in (F). Black numbers indicate beginning and ending amino acid residues of pericentrin A and B. Light blue numbers indicate construct identity and correspond to lane labels in (F). Yellow stars mark construct 7, which was found to IP endogenous Cdk5rap2.

(E) Cells were transfected with Flag constructs and extracts were subjected to Flag IP followed by pericentrin western blot (top). Second blot from top is pericentrin western of whole-cell extracts. Third and fourth blots from top are Flag western of whole-cell extracts. Extracts were run on two separate gels with different acrylamide percentages because of the difference in protein product size.

(F) Cells were transfected with either HA vector (Vector) or HA-pericentrin constructs 1 through 10, and extracts were subjected to HA IP and Cdk5rap2 western blot (top). Middle: Cdk5rap2 western blot of whole-cell extract. Bottom: HA Western of whole-cell extract.

Table 1. Identification of Bands from Cdk5rap2 IP/Mass Spectrometry Screen

Band Number	Approximate Band Size (kDa)	Mass Spec Identification	Expected Size (kDa)	Top Blast Matches
1	>250	Unnamed Protein BAE26362.1	135	Pericentrin (~320 kDa)
2	250	mKIAA1633 protein	210	Cdk5rap2 (~200 kDa)
3	160	mKIAA1633 protein	210	Cdk5rap2 (~200 kDa)
4	130	mKIAA1633 protein	210	Cdk5rap2 (~200 kDa)
5	95	mKIAA1633 protein (match #4)	210	Cdk5rap2 (~200 kDa)

Bands 1 through 5 correspond to numbered bands in Figure 6A. Mass Spec Identification column provides the top GenBank database match for each band analyzed. Protein sequences of these matches were analyzed by protein BLAST to identify full-length protein containing these sequences (Top BLAST Matches). Expected Size refers to the expected size of the original GenBank database match. Top BLAST Matches column provides the predicted size of the matching full-length protein in parentheses.

fragment 7c was sufficient to coIP endogenous Cdk5rap2 (Figure S7D). This suggests that Cdk5rap2 interacts with domains exclusive to pericentrin B. This is interesting given that both isoforms are expressed strongly in brain tissue at early stages of development (Figure S7E).

We also cotransfected cells with Cdk5rap2 construct 6b (Flag6b) and pericentrin construct 7 (HAP7) and found that each construct could coIP the other (Figure 6G). This confirms that both domains interact directly or through association with the same protein complex.

Pericentrin Knockdown Phenocopies Effects of Cdk5rap2 Knockdown on Neurogenesis

Given that Cdk5rap2 associates with pericentrin, we looked for evidence of a functional interaction between these proteins in the context of neurogenesis. Specifically, we asked whether depletion of pericentrin in cells of the developing neocortex might result in similar changes as observed following Cdk5rap2 depletion. We first asked whether knockdown of pericentrin levels by in utero electroporation of a small hairpin targeting pericentrin (shP1, Figure S8A) could mimic the effects of Cdk5rap2 knockdown on cell distribution between different cortical layers. Indeed, knockdown of pericentrin resulted in a similar redistribution of electroporated cells (Figure 7A, panels i, ii, and iii). Compared with control samples, knockdown of pericentrin resulted in fewer cells remaining within the VZ/SVZ and more cells localized to the IZ and CP (Figure 7B; control, n = 3; shP1, n = 5). We were able to rescue this defect via overexpression of Kendrin cDNA—the human pericentrin homolog—encoding mutations that resist targeting by shP1 (rescue) (Figure S8B and Figures 7D and 7F; all conditions, n = 3). Additionally, we found that overlap with Tuj1 signal was significantly increased following shP1 electroporation (Figure 7A, panel iv, and 7C; control, n = 3; shP1, n = 5). Thus, knockdown of pericentrin grossly phenocopies the effects of Cdk5rap2 depletion on cell redistribution and neuronal differentiation.

We also subjected shP1 electroporated brains to a 24 hr BrdU labeling paradigm beginning at E13.5. Pericentrin knockdown resulted in a reduced BrdU labeling index compared with controls (control and shP1, n = 3; Figures 7E, panels i, ii, and iv, and 7G). Additionally, we documented an increase in cell-cycle exit compared with controls (control and shP1, n = 3; Figures 7E and 7H). Thus, pericentrin knockdown mimics the effects of decreased Cdk5rap2 levels on cell proliferation and cell-cycle exit. This in turn suggests that the interaction between Cdk5rap2 and pericentrin is crucial for maintaining the progenitor pool during corticogenesis.

Pericentrin Recruits Cdk5rap2 to the Centrosome

Because Cdk5rap2 and pericentrin associate with one another and produce similar phenotypes in cortical cells upon knockdown, we wished to know how loss of either protein or disruption of their association affects the other at the cellular level. Given that both proteins display a centrosomal localization (Doxsey et al., 1994; Graser et al., 2007), we asked whether localization of either protein to the centrosome is dependent upon this interaction. Knockdown of pericentrin in U2OS cells results in depletion of centrosomal Cdk5rap2 signal whereas pericentrin and Cdk5rap2 are mutually dependent for their centrosomal accumulation in HeLa cells (Graser et al., 2007; Haren et al., 2009). We investigated this relationship in mouse NIH 3T3 cells. Knockdown of Cdk5rap2 using either of two constructs encoding shC1 or shC2 and a GFP expression sequence (Figure S7B) resulted in no significant change in the centrosome signal intensity of pericentrin compared to a control small hairpin expression directed against CD8 (all conditions, n = 6 coverslips; Figures 8A and 8B). We also tested the possibility that overexpression of Cdk5rap2 and pericentrin interaction domain fragments might disrupt interaction of the endogenous proteins and affect protein localization. Overexpression had no significant effect on centrosomal pericentrin signal intensity compared with controls (all conditions, n = 8; Figure 8C). We conclude that neither the presence of Cdk5rap2 nor the interaction with Cdk5rap2 is necessary for recruitment of pericentrin to the centrosome in NIH 3T3 cells.

On the other hand, when we looked at the effect of pericentrin knockdown on Cdk5rap2 centrosome signal intensity using either of two pericentrin knockdown constructs (shP1 and shP2, Figure S8A), we observed a significant reduction in signal intensity compared with control cells (control, n = 6; shP1, n = 6;

(G) Complementary coIP and western blot of HA-tagged pericentrin construct 7 (HAP7) and Flag-tagged Cdk5rap2 construct 6b (Flag6b). Cells were transfected with either HAP7 or HA vector (HA) and Flag6b or Flag vector (Flag). Cells extracts were subjected to Flag or HA IP (indicated by IP Set label) followed by western blot with HA or Flag antibody (indicated to right of blots). Top two blots: Flag (top) and HA (bottom) western blots of immunoprecipitated extracts. Bottom two blots: Flag (top) and HA (bottom) western blots of whole-cell extracts.

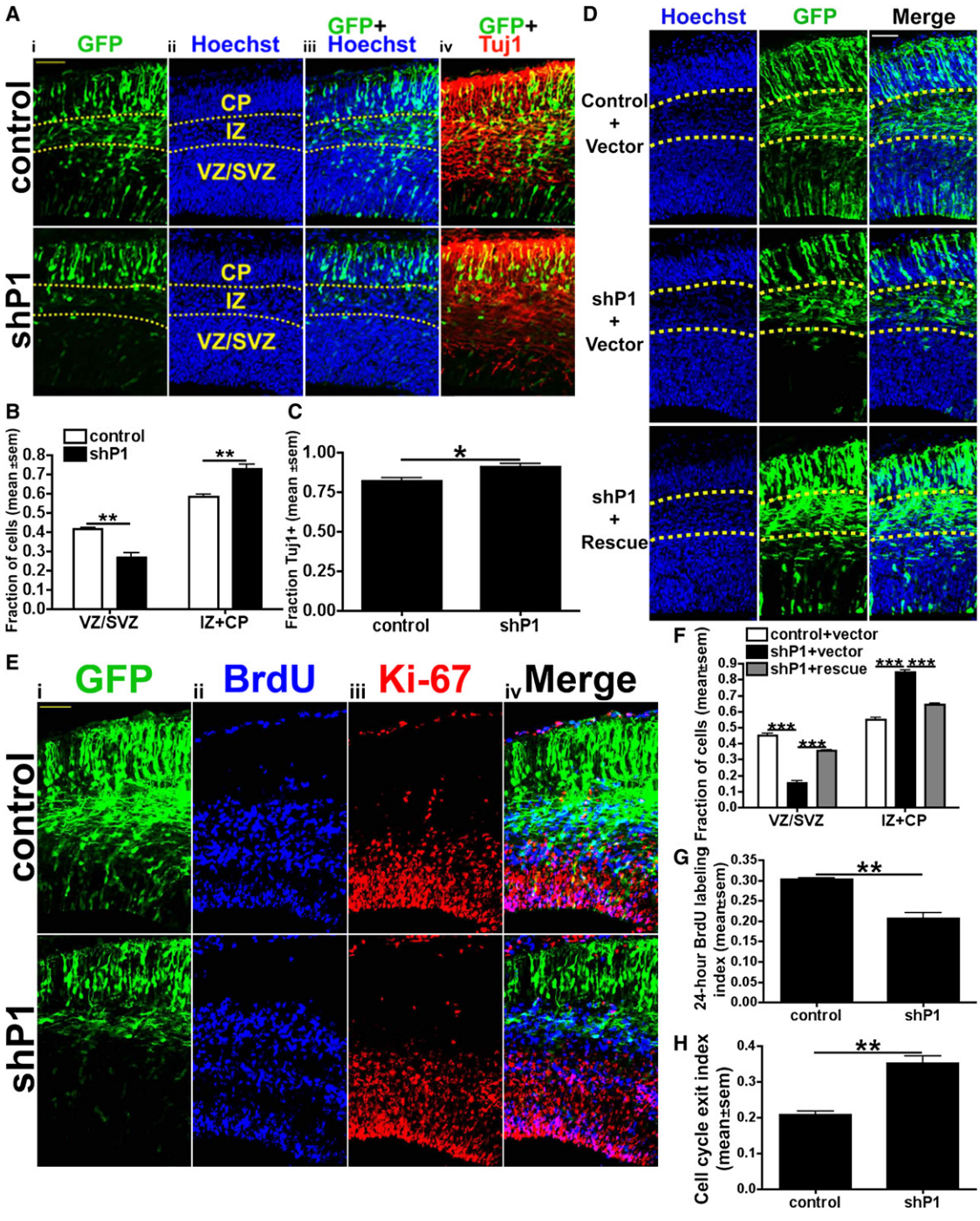

Figure 7. Knockdown of Pericentrin Phenocopies Effects of Cdk5rap2 Knockdown on Neurogenesis

(A) Images of brain sections coelectroporated with GFP expression plasmid and either control (top row) or shP1 (bottom row) constructs. Column i, GFP; column ii, Hoechst; column iii, merge of GFP and Hoechst; column iv, merge of GFP and Tuj1.

(B) Quantification of cell distribution between the VZ/SVZ and IZ + CP at E14.5 (t test).

(C) Quantification of fraction of GFP^+ cells that overlap with Tuj1 signal (t test).

(D) Images of brain sections electroporated with control hairpin and pCAX vector (top row), shP1 and pCAX vector (middle), or shP1 and Kendrin rescue construct (bottom). Hoechst, left column; GFP, middle column; merge, right column. Yellow dashed lines in panels (A) and (D) mark borders of different cortical zones.

(E) Images of brain section coelectroporated with GFP expression plasmid and either control (top row) or shP1 (bottom row). Cells were pulse-labeled with BrdU at E13.5 and harvested 24 hr later. Column i, GFP; column ii, BrdU; column iii, Ki67; column iv, merge of GFP, BrdU, and Ki67.

(F) Quantification of cell distribution between the VZ/SVZ and IZ + CP at E14.5. One-way ANOVA.

shP2, n = 4; Figures 8D and 8E). Cdk5rap2 levels also decreased significantly following overexpression of the interaction domains (all conditions, n = 8; Figure 8F). These results confirm that pericentrin recruits Cdk5rap2 to the centrosome whereas reduced Cdk5rap2 expression or disruption of the pericentrin-Cdk5rap2 interaction has no observable effect on the concentration of pericentrin at the centrosome in NIH 3T3 cells.

We asked whether decreased pericentrin expression similarly affected recruitment of Cdk5rap2 to the centrosome in neural progenitor cells. We simultaneously measured Cdk5rap2 and pericentrin fluorescent signal intensity in apical cellular processes in the neocortex, following in utero electroporation of either control or shP1 constructs. Both Cdk5rap2 and pericentrin fluorescent signal intensity appeared weaker following pericentrin knockdown (magenta arrows, Figure 8G). Analysis of both mean pericentrin signal intensity and mean Cdk5rap2 signal intensity (control, n = 62 centrosomes from three brains; shP1, n = 66 centrosomes from three brains) indicated that knockdown of pericentrin resulted in decreased detectable pericentrin and Cdk5rap2 levels at the centrosome (Figures S9A and S9B). Moreover, pericentrin knockdown resulted in a correlated decrease in Cdk5rap2 and pericentrin signal intensity in individual cells (control, r = 0.7114; shP1, r = 0.6785), demonstrating that Cdk5rap2 recruitment to the centrosome is dependent upon pericentrin expression levels (Figure 8H). Thus, we conclude that while centrosomal recruitment of pericentrin is not dependent upon Cdk5rap2, recruitment of Cdk5rap2 to the centrosome is strongly dependent upon pericentrin expression in progenitor cells of the embryonic mouse neocortex. This finding demonstrates the significance of the relationship between Cdk5rap2 and pericentrin. Loss of this interaction results in a deficiency of critical centrosome-associated functions of Cdk5rap2 that ultimately result in defects in neurogenesis and cortical development (Figure 8I). Collectively, our results outline a mechanism relevant to MCPH and MOPDII in which the pericentrin-Cdk5rap2 interaction plays a crucial role in proper regulation and maintenance of the neural progenitor pool.

DISCUSSION

In this study we examine the role of Cdk5rap2 in neurogenesis. We show that Cdk5rap2 is expressed in the embryonic mammalian brain and that its expression is most robust during periods of active neurogenesis and in apical processes of progenitor cells within the neocortical VZ. Depletion of Cdk5rap2 in cells of the embryonic neocortex results in altered distribution of cells among cortical layers. This redistribution results from an increase in premature neuronal differentiation and cell-cycle exit compared with controls. We link the function of Cdk5rap2 in neurogenesis to its interaction with pericentrin, which recruits Cdk5rap2 to the centrosome in neural progenitors.

Cdk5rap2 is a centrosome protein and its mRNA transcript is expressed in proliferative regions of the developing brain (Andersen et al., 2003; Bond et al., 2005; Fong et al., 2008; Graser et al., 2007; Magdaleno et al., 2006). Neurogenesis proceeds from E11 to E19 in the mouse, coinciding with a period of robust Cdk5rap2 expression in the brain. Interestingly, we observe a switch in Cdk5rap2 isoform expression commencing between E15.5 and E17.5, around the final days of neocortical neurogenesis. These alternative isoforms may be specific to postmitotic cells, as they persist in expression following the end of neurogenesis and we observe Cdk5rap2 expression in postmitotic cells. Although the function of Cdk5rap2 in postmitotic cells is not clear, it is possible that it plays a role in other centrosome-associated functions such as microtubule nucleation that remain important after cell-cycle exit. On the other hand, initial expression of these smaller isoforms coincides with the onset of gliogenesis and may represent glial-specific isoforms.

We have characterized a functional interaction between Cdk5rap2 and pericentrin. We find that the proteins associate via the extreme carboxy terminal region of Cdk5rap2 and a central region of pericentrin. Previous work has demonstrated that Cdk5rap2 binds to γ tubulin via its amino terminus and that this region associates with multiple components of the γTuRC (Fong et al., 2008). Pericentrin interacts with multiple γTuRC proteins to anchor the γTuRC at the centrosome, and disrupting this interaction or depletion of pericentrin results in abnormal mitotic spindle formation (Dictenberg et al., 1998; Rauch et al., 2008; Zimmerman et al., 2004). It is notable that the Cdk5rap2 domain of interaction with pericentrin lies at the extreme opposite end of the protein from its γ tubulin interaction domain. This suggests the possibility that Cdk5rap2 acts as a bridge between pericentrin and γ tubulin.

Interestingly, overexpression of either domain in cultured cells had only a small but significant effect upon Cdk5rap2 recruitment to the centrosome, and in vivo overexpression produced no discernible effects upon progenitor proliferation or neuronal differentiation (data not shown). This lack of a more dramatic effect may result from decreased stability or abnormal trafficking of the isolated protein domains. However, it is also possible that other proteins which associate with both Cdk5rap2 and pericentrin are able to maintain Cdk5rap2 localization at the centrosome via a separate interaction with pericentrin. Such a scenario would explain why depletion of pericentrin itself results in dramatic decreases in Cdk5rap2 at the centrosome while disruption of the Cdk5rap2-pericentrin association via domain overexpression produces only minor changes in Cdk5rap2 recruitment.

Our results demonstrate that localization of Cdk5rap2 to the centrosome in neural progenitor cells is dependent upon pericentrin. This also appears to be the case in cultured NIH 3T3 and U2OS cells, but not in HeLa cells (Graser et al., 2007; Haren et al., 2009). A number of PCM and γTuRC-associated proteins appear to be necessary for recruitment of the γTuRC to the centrosome and subsequent stabilization and anchoring of microtubules (Lüders and Stearns, 2007; Raynaud-Messina and Merdes, 2007). The fact that γ tubulin levels are affected by pericentrin depletion mainly in mitotic cells suggests the possibility that pericentrin may play a specialized role in

(G) Quantification of 24 hr BrdU labeling index (t test).
(H) Quantification of cell cycle exit index (t test).
For all graphs: mean ± SEM; *p < 0.05; **p < 0.01; ***p < 0.001. All scale bars = 50 μm.

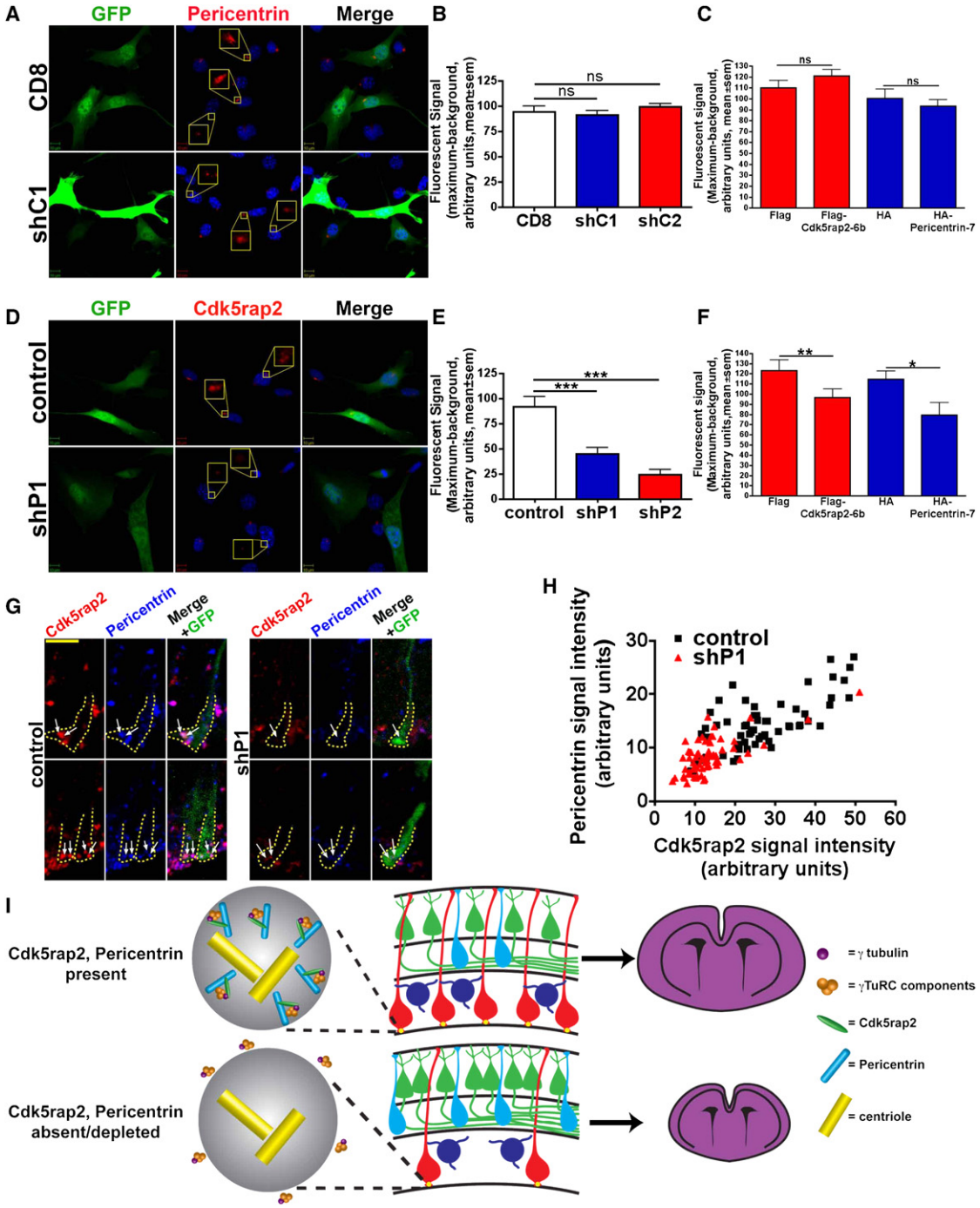

Figure 8. Pericentrin Recruits Cdk5rap2 to the Centrosome

(A) Images of NIH 3T3 cells that coexpress GFP and either a negative control (CD8, top row) or shC1 (bottom row), stained for pericentrin. Left column, GFP; middle row, Hoechst and pericentrin; right column, merge. Scale bars = 10 μm. Yellow boxes show zoomed images of centrosome signal.

(B) Quantification of maximum centrosomal pericentrin fluorescent signal intensity following Cdk5rap2 knockdown. Mean ± SEM; ns, $p > 0.05$, one-way ANOVA.

(C) Quantification of maximum centrosomal pericentrin fluorescent signal intensity following overexpression of Cdk5rap2 and pericentrin interaction domain expression constructs. Mean ± SEM; ns, $p > 0.05$, t test.

(D) Images of NIH 3T3 cells cotransfected with GFP expression plasmid and either control (top row) or shP1 (bottom row) construct, stained for Cdk5rap2 immunofluorescence. Left column, GFP; middle row, Hoechst and Cdk5rap2; right column, merge. Scale bars = 10 μm.

(E) Quantification of maximum centrosomal Cdk5rap2 fluorescent signal intensity, following pericentrin knockdown. Mean ± SEM; ***$p < 0.001$, one-way ANOVA.

(F) Quantification of maximum centrosomal Cdk5rap2 fluorescent signal intensity following overexpression of Cdk5rap2 and pericentrin interaction domain expression constructs. Mean ± SEM; **$p < 0.01$. *$p < 0.05$ (t test).

recruiting γTuRC via its interaction with Cdk5rap2 during this stage of the cell cycle (Zimmerman et al., 2004). In future studies it will be important to define the function of both pericentrin and Cdk5rap2 at the centrosome with respect to different phases of the cell cycle.

The exact cellular mechanism by which MCPH arises remains unknown. Every protein implicated in MCPH has been reported to display centrosomal localization (Cox et al., 2006; Pfaff et al., 2007; Xu et al., 2004; Zhong et al., 2006). This points to a central role for the centrosome and its associated structures in the cellular process disrupted by MCPH-associated mutations. The astral microtubules affected by Cdk5rap2 knockdown are postulated to play an important role in determining spindle orientation through contact with the cell cortex, which is thought to have implications for daughter cell fate in neural progenitors (Buchman and Tsai, 2007). Previous work has demonstrated that Aspm expression is a determinant of cleavage plane orientation and cell fate, supporting the idea that altered daughter cell identity due to changes in neural progenitor cleavage plane orientation are a probable cause of MCPH (Fish et al., 2006).

Our study uncovers another potential mechanism to explain depletion of the progenitor pool within the context of MCPH. Specifically, we find that Cdk5rap2 knockdown alters the makeup of the progenitor pool itself, decreasing the relative proportion of apical progenitors and increasing the relative proportion of basal progenitors. This shift is also supported by the increase in nonsurface mitoses observed following Cdk5rap2 knockdown. Apical progenitors have the capacity to self-renew and maintain the progenitor pool during neurogenesis. The vast majority of basal progenitors undergo a single terminal neurogenic division (Noctor et al., 2008). Thus, any decrease in the tendency of apical progenitors to undergo self-renewing divisions would be predicted to lead to a rapid depletion of the progenitor pool. On the other hand, an increase in the proportion of basal progenitors would lead to a transient increase in neuronal output. The change we observe most likely represents an increased failure of apical progenitors to commit to asymmetric self-renewing and proliferative divisions and a bias toward divisions that produce more basal progenitors and neurons that lack the capacity to repopulate the progenitor pool. Our data probably capture a snapshot of the progenitor pool at a time point during which a large number of apical progenitors have undergone non-self-renewing divisions that generate basal progenitors and neurons, leading to a transient burst in neurogenesis at the expense of maintaining the overall progenitor pool. This is in contrast to an alternative scenario where such a shift in progenitor pool makeup could signal a true increase in basal progenitor production, leading to a marked and more enduring increase in neurogenesis. It is worth noting that single-nucleotide polymorphisms of *CDK5RAP2* associated with MCPH in males are correlated with a decrease in cortical area, a finding that agrees with a primary effect of Cdk5rap2 knockdown on proliferation of radial glia (Rimol et al., 2010).

Other mechanisms may also contribute to progenitor pool depletion following Cdk5rap2 knockdown. For instance, the fact that we observe increased numbers of nonsurface mitoses opens the possibility of defects in interkinetic nuclear migration. Defects in this aspect of neural progenitor behavior have previously been associated with progenitor depletion (Xie et al., 2007; Zhang et al., 2009). We also observed that Cdk5rap2 knockdown resulted in altered cell-cycle dynamics in cultured N2A and neural progenitor cells. We specifically found that the fraction of N2A cells forming the G0/G1 population was increased upon Cdk5rap2 knockdown, suggestive of an increase in G1 length. Because increasing G1 length is associated with neuronal differentiation, this suggests another potential mechanism through which Cdk5rap2 may regulate neurogenesis and progenitor maintenance (Calegari and Huttner, 2003; Takahashi et al., 1995). Thus, Cdkrap2 knockdown could potentially lead to progenitor pool depletion by driving neural progenitors toward terminal neurogenic divisions as a result of increased G1 length.

Interestingly, recent work has described microcephaly and an overall growth defect in both a pericentrin hypomorph and a separate mouse line encoding a frameshift mutation that results in undetectable levels of pericentrin (Endoh-Yamagami et al., 2010; Miyoshi et al., 2009). In the latter mouse model, cortical thickness is reduced and BrdU-labeled cells are abnormally distributed after 3 days, with fewer cells in the VZ and more cells in the CP compared with control mice. The authors detail a significant increase in CC3 staining in mutant mice, and apoptosis probably accounts in part for the decreased cortical thickness. However, it seems likely that other mechanisms such as premature cell-cycle exit may play a role in the mutant phenotype, in line with our own observations.

Both Cdk5rap2 and pericentrin are implicated in human genetic diseases—MCPH and MOPDII—that include microcephaly as part of their disease phenotypes (Bond et al., 2005; Rauch et al., 2008). MCPH and MOPDII differ, however, in several respects. Manifestation of microcephaly in MCPH patients is established during prenatal growth, whereas in MOPDII an overall intrauterine growth defect results in individuals being born with a head circumference that is below average but normal relative to overall body size (Woods et al., 2005). This is followed by decelerated head growth after birth, a feature absent in MCPH (Hall et al., 2004). The majority of MCPH patients do not exhibit

(G) Images of apical cell processes 72 hr following in utero coelectroporation with a GFP expression plasmid and either control or shP1. Left columns, Cdk5rap2 signal; middle columns, pericentrin signal; right columns, merge plus GFP. Dashed yellow lines outline the edge of apical processes. Arrows identify true centrosomal signal of each apical process. Ventricle is down. Scale bar = 5 μm.

(H) X-Y scatter plot depicting mean Cdk5rap2 versus mean pericentrin signal per centrosome, 72 hr after electroporation of control (■) or shP1 (▲) constructs. X-Y correlation analysis: control, $p < 0.0001$, $r = 0.7114$; shP1: $p < 0.0001$, $r = 0.6785$.

(I) Model of Cdk5rap2 and pericentrin function in neurogenesis and microcephaly. Cdk5rap2 and pericentrin recruit γTuRC to the centrosome (left), resulting in a balance between proliferation and differentiation of neural progenitors (middle) and ultimately production of a normal brain at birth (right). In the absence of Cdk5rap2 and pericentrin (bottom), the γTuRC is not efficiently recruited to the centrosome (left), resulting in increased neuronal differentiation and depletion of the progenitor pool (middle). This ultimately results in microcephaly with a pronounced effect on the neocortex (right).

severe growth defects. MOPDII patients, on the other hand, usually reach a total height of ~100 cm, and exhibit a host of other developmental abnormalities.

Primary microcephaly is the most notable common feature of these diseases. Our data complement current hypotheses about the origins of MCPH—namely that a defect in neural progenitor proliferation can account for the manifestation of primary microcephaly (Aicardi, 1998; Bond and Woods, 2006; Cox et al., 2006; Fish et al., 2006; Woods et al., 2005). We emphasize that initiating knockdown at early time points during neurogenesis in the neocortex is a particularly well-suited strategy for the study of MCPH as it allows us to target the cell population thought to be most involved in the manifestation of MCPH within the most severely affected region of the CNS. Our results additionally demonstrate that depletion of pericentrin can phenocopy many of the effects of Cdk5rap2, highlighting a common effect on neural progenitor proliferation between the two proteins. This points to what may be a common mechanism of reduced cellularity in the CNS observed in both diseases.

EXPERIMENTAL PROCEDURES

DNA Constructs

Flag-tagged Cdk5rap2 expression constructs were created by cloning Cdk5rap2 cDNA sequences into a pCDNA3 vector with two myc and three Flag epitope sequences. Flag-ATF4 construct was cloned into the same vector. HA-tagged pericentrin domain expression constructs were created by cloning pericentrin cDNA sequences into a modified pEGFP-C1 plasmid where EGFP coding sequence was replaced by three HA coding sequences. Composition of individual constructs is detailed in Supplemental Experimental Procedures.

Small hairpin constructs were cloned into either pSilencer 2.0-U6 (Ambion, Austin) or pLentiLox 3.7 (Rubinson et al., 2003). All small hairpin sequences except shP1 were designed using the Genscript siRNA Target Finder. shP1 was based on a published sequence (Dammermann and Merdes, 2002). Details of small hairpin targeting sequences are listed in Supplemental Experimental Procedures.

Cdk5rap2 Antibody Production

A His-tagged construct encoding residues 1 through 431 of the Cdk5rap2 sequence was cloned into the pET-21a vector. Purified protein was concentrated and injected into rabbits by PRF&L for antibody production. Antibody was purified from rabbit serum against a GST tagged construct expressing the first 320 amino acids of the Cdk5rap2 sequence.

CoIP Assays

N2A cells were transfected using Lipofectamine 2000 transfection reagent (Invitrogen) and allowed to incubate for 24 to 48 hr. Cells were lysed in buffer containing 250 mM NaCl, 50 mM Tris (pH7.5), 5 mM EDTA, 0.1% Igepal CA-630 (Sigma), 1,4 dithiothreitol (DTT), protease inhibitor cocktail tablet (Roche, Basel), and phosphatase inhibitors. Extracts were incubated with either anti-Flag M2 affinity gel or anti-HA agarose beads (Sigma), washed, and run out on polyacrylamide gels before protein transfer and western detection.

Cdk5rap2 Immunoprecipitation Followed by Mass Spectrometry

Whole-brain extracts of E11.5 mice were collected by Dounce homogenization of tissue and lysis in buffer: 150 mM NaCl, 50 mM Tris (pH 8.0), 0.1%SDS, 12 mM sodium deoxycholate, and 1% Igepal CA-630 (Sigma). Precleared extracts were incubated with protein A and G sepharose beads (GE Healthcare, Piscataway, NJ) bound to either preimmune serum or Cdk5rap2 antibody. Beads were washed in lysis buffer and bound protein was collected and run on a 10% polyacrylamide gel. The separated proteins were visualized with SimplyBlue SafeStain (Invitrogen), and in-gel digestion with DTT reduction-iodoacetamide alkylation-trypsin was performed. Tryptic digests were extracted and analyzed by iron-trap tandem mass spectrometry. The iron-trap tandem mass spectrometry was carried out in a LCQ Deca XP coupled to a microspray Vydac C18 column HPLC system and operated by Xcalibure 1.2 XP1 software. Peak lists acquired by mass spectrometer were analyzed by BioWorks 3.1.

In Utero Electroporation

In utero electroporation was performed as described elsewhere (Xie et al., 2007). Small hairpin plasmid DNA and GFP expression plasmid DNA were mixed in a 3:1 ratio at a total concentration of 1 mg/ml in solution. Fluorescent labeling of electroporated cells was achieved using a pCAGIG plasmid (Matsuda and Cepko, 2004) modified by insertion of a Venus YFP sequence into the MCS. All electroporations were performed at E11.5 and brains were harvested between E13.5 and P6. For BrdU labeling experiments, pregnant dams were injected with 1 ml 2 mg/ml BrdU solution at either E13.5 or E14.5.

Preparation of Cells and Tissue for Immunofluorescent Staining

Dissociated cells were fixed in 4% paraformaldehyde (PFA)/phosphate-buffered saline (PBS) solution for 4 min at room temperature, washed with PBS, blocked in 3% bovine serum albumin/10% goat serum/0.2% Triton/PBS solution, and stained in blocking solution with antibody. Embryonic brains were prepared for staining either by cardiac perfusion with PFA or drop fixation into 4% PFA solution. Perfused brains were embedded in agar and sectioned via vibratome. Drop-fixed brains were frozen in Tissue-Tek embedding medium (Sakura, Torrance, CA) and sectioned via cryostat. Brain sections were stained under conditions similar to those used for dissociated cells. Sections stained for BrdU detection were subject to 3 hr treatment with 2N HCl prior to blocking.

Analysis of Brain Sections

Distribution of electroporated cells between cortical zones was evaluated on the basis of zone divisions as determined by Hoechst staining. To determine overlap of GFP cells with Tuj1 staining in brain sections, we first counted all GFP^+ cells in the section. Because Tuj1 signal is ubiquitous in the IZ and CP, we counted all cells in these layers as $Tuj1^+$. Cells in the SVZ that lay within this region of ubiquitous Tuj1 staining were counted as positive. Cells in the SVZ below this region and those cells in the VZ were evaluated for Tuj1 signal overlap on an individual basis. The cell-cycle exit index was calculated as the fraction of all GFP, BrdU double-positive cells minus the population of GFP, BrdU, Ki67 triple-positive cells over the entire GFP, BrdU double-positive population.

Evaluation of Centrosome Signal in NIH 3T3 Cells

For evaluation of pericentrin signal, cells were transfected with either pLL3.7 constructs encoding CD8, shC1, or shC2 and GFP sequences. For evaluation of Cdk5rap2 signal, cells were cotransfected with pSilencer constructs encoding control, shP1, or shP2 and pEGFP-C1 (Clontech, Mountain View, CA). Images were taken by confocal microscopy 72 hr posttransfection. Maximal signal intensity was measured in 25 to 50 individual cells per coverslip using the LSM 510 software profile function and subtracting background intensity. For evaluation of signal intensity following expression of domain fragments, cells were transfected with appropriate constructs and fixed at 48 hr. Maximal signal intensity was determined as above. We used NIH 3T3 cells because they are a murine cell line susceptible to knockdown by our small hairpins and they reliably produce a clear centrosome signal.

Evaluation of Centrosome Signal in Electroporated Brain Sections

E14.5 brain sections electroporated at E11.5 were stained for pericentrin and Cdk5rap2 signal as described. Stacked images of apical processes from GFP^+ cells were collected at 100X magnification on a confocal microscope. To determine which centrosome signal belonged to an individual apical process, individual image layers were evaluated for GFP signal and overlap with centrosome protein signal. The corresponding image layers were stacked using the max intensity setting in ImageJ. The ImageJ ROI manager was then used to simultaneously measure the average signal intensity of pericentrin and Cdk5rap2 signal in two equal-sized regions covering the centrosome signal

and a background region. The difference in average signal intensity determined our final measure of signal intensity.

Microscopy

All images were captured using either a Zeiss LSM 510 confocal microscope and LSM 510 software or a Nikon Eclipse TE300 inverted epifluorescent microscope and Openlab software.

Data Analysis

All data were analyzed using Prism software (GraphPad Software, Inc, La Jolla, CA). Tests used were two-tailed t test, one-way analysis of variance paired with Tukey post-test, and Pearson linear correlation analysis.

SUPPLEMENTAL INFORMATION

Supplemental Information includes nine figures and Supplemental Experimental Procedures and can be found with this article online at doi:10.1016/j.neuron.2010.03.036.

ACKNOWLEDGMENTS

We would like to thank Y. Mao, K. Singh, and D. Kim for helpful comments and criticism of the manuscript. Thanks to X. Ge for preparing and contributing perfused embryonic brains. Thanks to Dr. Stephen Doxsey for providing human Kendrin cDNA. The Pax6 antibody developed by A. Kawakami was obtained from the Developmental Studies Hybridoma Bank developed under the auspices of the NICHD and maintained by The University of Iowa, Department of Biology, Iowa City, IA 52242. This work was supported by grant NS37007 from the National Institutes of Health. L.-H.T. is an investigator of the Howard Hughes Medical Institute and the director of the neurobiology program at the Stanley Center for Psychiatric Research.

Accepted: March 11, 2010
Published: May 12, 2010

REFERENCES

Aicardi, J. (1998). Diseases of the Nervous System in Childhood, Second Edition (London: Mac Keith Press).

Andersen, J.S., Wilkinson, C.J., Mayor, T., Mortensen, P., Nigg, E.A., and Mann, M. (2003). Proteomic characterization of the human centrosome by protein correlation profiling. Nature *426*, 570–574.

Angevine, J.B., Jr., and Sidman, R.L. (1961). Autoradiographic study of cell migration during histogenesis of cerebral cortex in the mouse. Nature *192*, 766–768.

Bond, J., and Woods, C.G. (2006). Cytoskeletal genes regulating brain size. Curr. Opin. Cell Biol. *18*, 95–101.

Bond, J., Roberts, E., Mochida, G.H., Hampshire, D.J., Scott, S., Askham, J.M., Springell, K., Mahadevan, M., Crow, Y.J., Markham, A.F., et al. (2002). ASPM is a major determinant of cerebral cortical size. Nat. Genet. *32*, 316–320.

Bond, J., Roberts, E., Springell, K., Lizarraga, S.B., Lizarraga, S., Scott, S., Higgins, J., Hampshire, D.J., Morrison, E.E., Leal, G.F., et al. (2005). A centrosomal mechanism involving CDK5RAP2 and CENPJ controls brain size. Nat. Genet. *37*, 353–355.

Buchman, J.J., and Tsai, L.H. (2007). Spindle regulation in neural precursors of flies and mammals. Nat. Rev. Neurosci. *8*, 89–100.

Busson, S., Dujardin, D., Moreau, A., Dompierre, J., and De Mey, J.R. (1998). Dynein and dynactin are localized to astral microtubules and at cortical sites in mitotic epithelial cells. Curr. Biol. *8*, 541–544.

Calegari, F., and Huttner, W.B. (2003). An inhibition of cyclin-dependent kinases that lengthens, but does not arrest, neuroepithelial cell cycle induces premature neurogenesis. J. Cell Sci. *116*, 4947–4955.

Cox, J., Jackson, A.P., Bond, J., and Woods, C.G. (2006). What primary microcephaly can tell us about brain growth. Trends Mol. Med. *12*, 358–366.

Dammermann, A., and Merdes, A. (2002). Assembly of centrosomal proteins and microtubule organization depends on PCM-1. J. Cell Biol. *159*, 255–266.

de Anda, F.C., Pollarolo, G., Da Silva, J.S., Camoletto, P.G., Feiguin, F., and Dotti, C.G. (2005). Centrosome localization determines neuronal polarity. Nature *436*, 704–708.

Desir, J., Cassart, M., David, P., Van Bogaert, P., and Abramowicz, M. (2008). Primary microcephaly with ASPM mutation shows simplified cortical gyration with antero-posterior gradient pre- and post-natally. Am. J. Med. Genet. A. *146A*, 1439–1443.

Dictenberg, J.B., Zimmerman, W., Sparks, C.A., Young, A., Vidair, C., Zheng, Y., Carrington, W., Fay, F.S., and Doxsey, S.J. (1998). Pericentrin and gamma-tubulin form a protein complex and are organized into a novel lattice at the centrosome. J. Cell Biol. *141*, 163–174.

Doxsey, S. (2001). Re-evaluating centrosome function. Nat. Rev. Mol. Cell Biol. *2*, 688–698.

Doxsey, S.J., Stein, P., Evans, L., Calarco, P.D., and Kirschner, M. (1994). Pericentrin, a highly conserved centrosome protein involved in microtubule organization. Cell *76*, 639–650.

Endoh-Yamagami, S., Karkar, K.M., May, S.R., Cobos, I., Thwin, M.T., Long, J.E., Ashique, A.M., Rubenstein, J.L., and Peterson, A.S. (2010). A mutation in the pericentrin gene causes abnormal interneuron migration to the olfactory bulb in mice. Dev Biol. *340*, 41–53.

Farkas, L.M., and Huttner, W.B. (2008). The cell biology of neural stem and progenitor cells and its significance for their proliferation versus differentiation during mammalian brain development. Curr. Opin. Cell Biol. *20*, 707–715.

Faulkner, N.E., Dujardin, D.L., Tai, C.Y., Vaughan, K.T., O'Connell, C.B., Wang, Y., and Vallee, R.B. (2000). A role for the lissencephaly gene LIS1 in mitosis and cytoplasmic dynein function. Nat. Cell Biol. *2*, 784–791.

Ferland, R.J., Cherry, T.J., Preware, P.O., Morrisey, E.E., and Walsh, C.A. (2003). Characterization of Foxp2 and Foxp1 mRNA and protein in the developing and mature brain. J. Comp. Neurol. *460*, 266–279.

Fish, J.L., Kosodo, Y., Enard, W., Pääbo, S., and Huttner, W.B. (2006). Aspm specifically maintains symmetric proliferative divisions of neuroepithelial cells. Proc. Natl. Acad. Sci. USA *103*, 10438–10443.

Fong, K.W., Choi, Y.K., Rattner, J.B., and Qi, R.Z. (2008). CDK5RAP2 is a pericentriolar protein that functions in centrosomal attachment of the gamma-tubulin ring complex. Mol. Biol. Cell *19*, 115–125.

Graser, S., Stierhof, Y.D., and Nigg, E.A. (2007). Cep68 and Cep215 (Cdk5rap2) are required for centrosome cohesion. J. Cell Sci. *120*, 4321–4331.

Hall, J.G., Flora, C., Scott, C.I., Jr., Pauli, R.M., and Tanaka, K.I. (2004). Majewski osteodysplastic primordial dwarfism type II (MOPD II): natural history and clinical findings. Am. J. Med. Genet. A. *130A*, 55–72.

Haren, L., Stearns, T., and Lüders, J. (2009). Plk1-dependent recruitment of gamma-tubulin complexes to mitotic centrosomes involves multiple PCM components. PLoS ONE *4*, e5976.

Hassan, M.J., Khurshid, M., Azeem, Z., John, P., Ali, G., Chishti, M.S., and Ahmad, W. (2007). Previously described sequence variant in CDK5RAP2 gene in a Pakistani family with autosomal recessive primary microcephaly. BMC Med. Genet. *8*, 58.

Higginbotham, H.R., and Gleeson, J.G. (2007). The centrosome in neuronal development. Trends Neurosci. *30*, 276–283.

Jackson, A.P., McHale, D.P., Campbell, D.A., Jafri, H., Rashid, Y., Mannan, J., Karbani, G., Corry, P., Levene, M.I., Mueller, R.F., et al. (1998). Primary autosomal recessive microcephaly (MCPH1) maps to chromosome 8p22-pter. Am. J. Hum. Genet. *63*, 541–546.

Jamieson, C.R., Govaerts, C., and Abramowicz, M.J. (1999). Primary autosomal recessive microcephaly: homozygosity mapping of MCPH4 to chromosome 15. Am. J. Hum. Genet. *65*, 1465–1469.

Jamieson, C.R., Fryns, J.P., Jacobs, J., Matthijs, G., and Abramowicz, M.J. (2000). Primary autosomal recessive microcephaly: MCPH5 maps to 1q25-q32. Am. J. Hum. Genet. *67*, 1575–1577.

Jurczyk, A., Gromley, A., Redick, S., San Agustin, J., Witman, G., Pazour, G.J., Peters, D.J., and Doxsey, S. (2004). Pericentrin forms a complex with intraflagellar transport proteins and polycystin-2 and is required for primary cilia assembly. J. Cell Biol. *166*, 637–643.

Kumar, A., Girimaji, S.C., Duvvari, M.R., and Blanton, S.H. (2009). Mutations in STIL, encoding a pericentriolar and centrosomal protein, cause primary microcephaly. Am. J. Hum. Genet. *84*, 286–290.

Leal, G.F., Roberts, E., Silva, E.O., Costa, S.M., Hampshire, D.J., and Woods, C.G. (2003). A novel locus for autosomal recessive primary microcephaly (MCPH6) maps to 13q12.2. J. Med. Genet. *40*, 540–542.

Lüders, J., and Stearns, T. (2007). Microtubule-organizing centres: a re-evaluation. Nat. Rev. Mol. Cell Biol. *8*, 161–167.

Magdaleno, S., Jensen, P., Brumwell, C.L., Seal, A., Lehman, K., Asbury, A., Cheung, T., Cornelius, T., Batten, D.M., Eden, C., et al. (2006). BGEM: an in situ hybridization database of gene expression in the embryonic and adult mouse nervous system. PLoS Biol. *4*, e86.

Majewski, F., Ranke, M., and Schinzel, A. (1982). Studies of microcephalic primordial dwarfism II: the osteodysplastic type II of primordial dwarfism. Am. J. Med. Genet. *12*, 23–35.

Matsuda, T., and Cepko, C.L. (2004). Electroporation and RNA interference in the rodent retina in vivo and in vitro. Proc. Natl. Acad. Sci. USA *101*, 16–22.

Miyoshi, K., Kasahara, K., Miyazaki, I., Shimizu, S., Taniguchi, M., Matsuzaki, S., Tohyama, M., and Asanuma, M. (2009). Pericentrin, a centrosomal protein related to microcephalic primordial dwarfism, is required for olfactory cilia assembly in mice. FASEB J. *23*, 3289–3297.

Moynihan, L., Jackson, A.P., Roberts, E., Karbani, G., Lewis, I., Corry, P., Turner, G., Mueller, R.F., Lench, N.J., and Woods, C.G. (2000). A third novel locus for primary autosomal recessive microcephaly maps to chromosome 9q34. Am. J. Hum. Genet. *66*, 724–727.

Noctor, S.C., Martínez-Cerdeño, V., and Kriegstein, A.R. (2008). Distinct behaviors of neural stem and progenitor cells underlie cortical neurogenesis. J. Comp. Neurol. *508*, 28–44.

Pattison, L., Crow, Y.J., Deeble, V.J., Jackson, A.P., Jafri, H., Rashid, Y., Roberts, E., and Woods, C.G. (2000). A fifth locus for primary autosomal recessive microcephaly maps to chromosome 1q31. Am. J. Hum. Genet. *67*, 1578–1580.

Pfaff, K.L., Straub, C.T., Chiang, K., Bear, D.M., Zhou, Y., and Zon, L.I. (2007). The zebra fish cassiopeia mutant reveals that SIL is required for mitotic spindle organization. Mol. Cell. Biol. *27*, 5887–5897.

Rauch, A., Thiel, C.T., Schindler, D., Wick, U., Crow, Y.J., Ekici, A.B., van Essen, A.J., Goecke, T.O., Al-Gazali, L., Chrzanowska, K.H., et al. (2008). Mutations in the pericentrin (PCNT) gene cause primordial dwarfism. Science *319*, 816–819.

Raynaud-Messina, B., and Merdes, A. (2007). Gamma-tubulin complexes and microtubule organization. Curr. Opin. Cell Biol. *19*, 24–30.

Rimol, L.M., Agartz, I., Djurovic, S., Brown, A.A., Roddey, J.C., Kähler, A.K., Mattingsdal, M., Athanasiu, L., Joyner, A.H., Schork, N.J., et al; Alzheimer's Disease Neuroimaging Initiative. (2010). Sex-dependent association of common variants of microcephaly genes with brain structure. Proc. Natl. Acad. Sci. USA *107*, 384–388.

Roberts, E., Jackson, A.P., Carradice, A.C., Deeble, V.J., Mannan, J., Rashid, Y., Jafri, H., McHale, D.P., Markham, A.F., Lench, N.J., and Woods, C.G. (1999). The second locus for autosomal recessive primary microcephaly (MCPH2) maps to chromosome 19q13.1-13.2. Eur. J. Hum. Genet. *7*, 815–820.

Roberts, E., Hampshire, D.J., Pattison, L., Springell, K., Jafri, H., Corry, P., Mannon, J., Rashid, Y., Crow, Y., Bond, J., and Woods, C.G. (2002). Autosomal recessive primary microcephaly: an analysis of locus heterogeneity and phenotypic variation. J. Med. Genet. *39*, 718–721.

Rubinson, D.A., Dillon, C.P., Kwiatkowski, A.V., Sievers, C., Yang, L., Kopinja, J., Rooney, D.L., Zhang, M., Ihrig, M.M., McManus, M.T., et al. (2003). A lentivirus-based system to functionally silence genes in primary mammalian cells, stem cells and transgenic mice by RNA interference. Nat. Genet. *33*, 401–406.

Takahashi, T., Nowakowski, R.S., and Caviness, V.S., Jr. (1995). The cell cycle of the pseudostratified ventricular epithelium of the embryonic murine cerebral wall. J. Neurosci. *15*, 6046–6057.

Tsai, L.H., and Gleeson, J.G. (2005). Nucleokinesis in neuronal migration. Neuron *46*, 383–388.

Woods, C.G., Bond, J., and Enard, W. (2005). Autosomal recessive primary microcephaly (MCPH): a review of clinical, molecular, and evolutionary findings. Am. J. Hum. Genet. *76*, 717–728.

Xie, Z., Sanada, K., Samuels, B.A., Shih, H., and Tsai, L.H. (2003). Serine 732 phosphorylation of FAK by Cdk5 is important for microtubule organization, nuclear movement, and neuronal migration. Cell *114*, 469–482.

Xie, Z., Moy, L.Y., Sanada, K., Zhou, Y., Buchman, J.J., and Tsai, L.H. (2007). Cep120 and TACCs control interkinetic nuclear migration and the neural progenitor pool. Neuron *56*, 79–93.

Xu, X., Lee, J., and Stern, D.F. (2004). Microcephalin is a DNA damage response protein involved in regulation of CHK1 and BRCA1. J. Biol. Chem. *279*, 34091–34094.

Yingling, J., Youn, Y.H., Darling, D., Toyo-Oka, K., Pramparo, T., Hirotsune, S., and Wynshaw-Boris, A. (2008). Neuroepithelial stem cell proliferation requires LIS1 for precise spindle orientation and symmetric division. Cell *132*, 474–486.

Zhang, X., Lei, K., Yuan, X., Wu, X., Zhuang, Y., Xu, T., Xu, R., and Han, M. (2009). SUN1/2 and Syne/Nesprin-1/2 complexes connect centrosome to the nucleus during neurogenesis and neuronal migration in mice. Neuron *64*, 173–187.

Zhong, X., Pfeifer, G.P., and Xu, X. (2006). Microcephalin encodes a centrosomal protein. Cell Cycle *5*, 457–458.

Zimmerman, W.C., Sillibourne, J., Rosa, J., and Doxsey, S.J. (2004). Mitosis-specific anchoring of gamma tubulin complexes by pericentrin controls spindle organization and mitotic entry. Mol. Biol. Cell *15*, 3642–3657.

Zmuda, J.F., and Rivas, R.J. (1998). The Golgi apparatus and the centrosome are localized to the sites of newly emerging axons in cerebellar granule neurons in vitro. Cell Motil. Cytoskeleton *41*, 18–38.